Robust and Versatile Coatings Engineered via Simultaneous Covalent and Noncovalent Interactions

Jiajing Zhou,[a],[b] Matthew Penna,[c] Zhixing Lin,[a] Yiyuan Han,[a] René P. M. Lafleur,[a] Yijiao Qu,[a] Joseph J. Richardson,[a] Irene Yarovsky,[c] Jesse V. Jokerst*[b],[d],[e], and Frank Caruso*[a]

[a] Dr. J. Zhou, Z. Lin, Dr. Y. Han, Dr. R. P. M. Lafleur, Y. Qu, Dr. J. J. Richardson, Prof. F. Caruso
ARC Centre of Excellence in Convergent Bio-Nano Science and Technology, and the Department of Chemical Engineering
The University of Melbourne
Parkville, Victoria 3010 (Australia)
E-mail: fcaruso@unimelb.edu.au

[b] Dr. J. Zhou, Prof. J. V. Jokerst
Department of NanoEngineering
University of California San Diego
9500 Gilman Dr., La Jolla, CA 92093 (USA)
E-mail: jjokerst@eng.ucsd.edu

[c] Dr. M. Penna, Prof. I. Yarovsky
School of Engineering
RMIT University
Melbourne, Victoria 3001 (Australia)

[d] Prof. J. V. Jokerst
Materials Science and Engineering Program
University of California San Diego
9500 Gilman Dr., La Jolla, CA 92093 (USA)
E-mail: jjokerst@eng.ucsd.edu

[e] Prof. J. V. Jokerst
Department of Radiology
University of California San Diego
9500 Gilman Dr., La Jolla, CA 92093 (USA)
E-mail: jjokerst@eng.ucsd.edu

Supporting information for this article is given via a link at the end of the document.

Abstract: Interfacial modular assembly has emerged as an adaptable strategy for engineering the surface properties of substrates in biomedicine, photonics, and catalysis. Herein, we report a versatile and robust coating (pBDT–TA), self-assembled from tannic acid (TA) and a self-polymerizing aromatic dithiol (i.e., benzene-1,4-dithiol, BDT), that can be engineered on diverse substrates with a precisely tuned thickness (5–40 nm) by varying the concentration of BDT used. The pBDT–TA coating is stabilized by covalent (disulfide) bonds and supramolecular (π–π) interactions, endowing the coating with high stability in various harsh aqueous environments across ionic strength, pH, temperature (e.g., 100 mM NaCl, HCl (pH 1) or NaOH (pH 13), and water at 100 °C), as well as surfactant solution (e.g., 100 mM Triton X-100) and biological buffer (e.g., Dulbecco's phosphate-buffered saline), as validated by experiments and simulations. Moreover, the reported pBDT–TA coating enables secondary reactions on the coating for engineering hybrid adlayers (e.g., ZIF-8 shells) via phenolic-mediated adhesion, and the facile integration of aromatic fluorescent dyes (e.g., rhodamine B) via π interactions without requiring elaborate synthetic processes.

Engineering materials by manipulating their surface chemistry provides promise in diverse applications including biomedicine, catalysis, optics, and gas separation.[1–7] A versatile surface functionalization strategy involves phenolic-based coatings, which display multiple interactions with various materials and are therefore widely applicable. For example, covalently crosslinked phenolics (e.g., polydopamine) have been extensively investigated for producing robust coatings.[8–12] More recently, attention has been directed toward noncovalent, metal-coordinated phenolic coatings owing to their rapid and facile synthesis, stimulus-responsiveness, and tunable composition.[13–15] However, those supramolecular coatings can disassemble in aqueous environments owing to the presence of noncovalent stabilizing forces (e.g., van der Waals interactions, electrostatic interactions, hydrogen bonding, metal coordination) in response to changes in the surroundings (e.g., ionic strength, pH, and temperature).[16–19] Such disassembly provides advantages with respect to designing adaptive and responsive materials (e.g., drug delivery systems in biomedicine)[20,21] but may provide challenges in applications that require long-term robustness and stability (e.g., imaging, separations, and catalysis).[22,23] Therefore, the development of robust (i.e., displaying long-term stability in diverse environments), modular (structural and

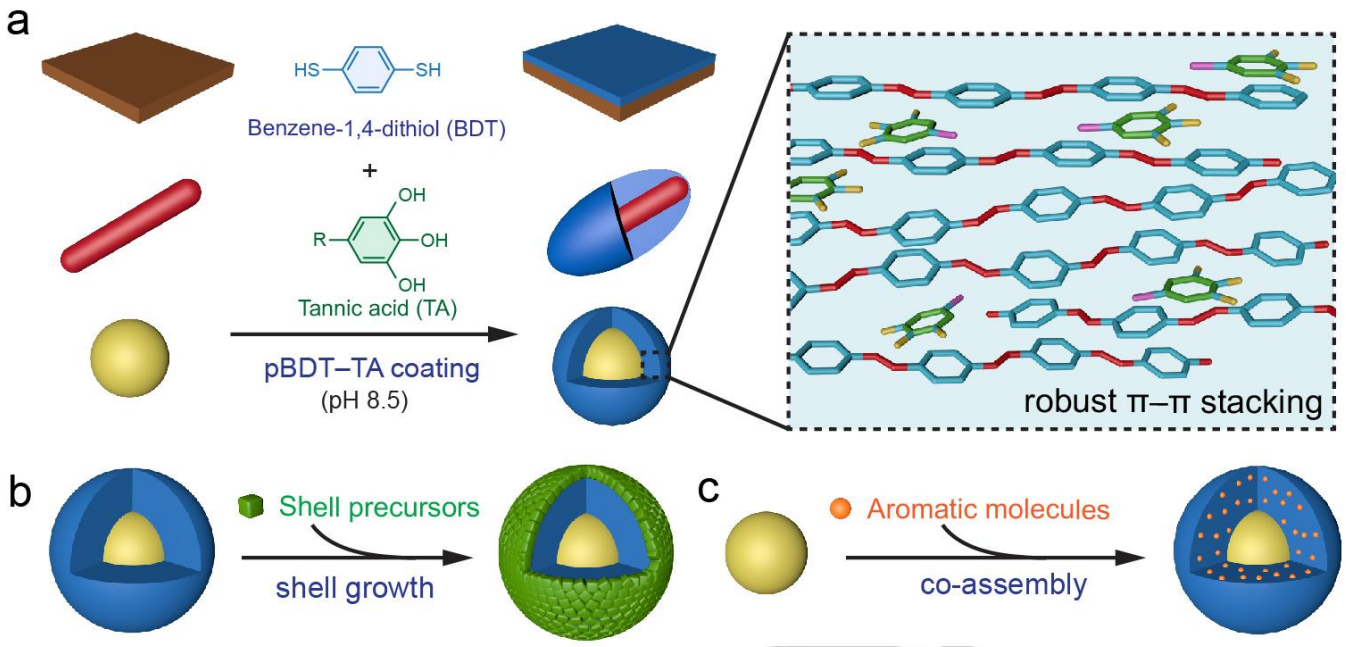

Figure 1. Surface engineering mediated by pBDT–TA coatings. (a) Schematic illustration of the assembly of pBDT–TA complexes on diverse substrates via covalent and noncovalent interactions. (b) Polyphenol-directed growth of diverse shell materials on preformed pBDT–TA coatings owing to the near-universal adhesion of phenolic groups. (c) Introduction of organic moieties (e.g., fluorescent dyes) into the pBDT–TA coating.

compositional flexibility), and adaptable (stimulus-responsiveness) materials is envisaged to broaden the applications of phenolic-based coatings.

Self-assembly processes are widely exploited for constructing structurally tunable and functional ensembles in nature, where the assembly process simultaneously involves covalent and noncovalent interactions among molecular units.[24,25] Inspired by this, we recently developed size-tunable nanoparticles (pBDT–TA) via the assembly of naturally available tannic acid (TA) and a self-polymerizable aromatic dithiol (i.e., benzene-1,4-dithiol, BDT)—the nanoparticles served as a generalizable particle template for synthesizing particles with various shell materials.[26] The presence of both covalent and noncovalent interactions in the pBDT–TA particles underpins their robust stability in various synthetic conditions. Therefore, we hypothesized that pBDT–TA complexes could serve as suitable coatings that would also exhibit the combined benefits of covalent and noncovalent interactions. The application of such pBDT–TA coatings would expand the library of phenolic-mediated coating strategies for engineering materials and surfaces.[27]

The interfacial assembly strategy for surface engineering using TA and BDT is shown in Figure 1a. Specifically, BDT first self-polymerizes into polybenzene-1,4-dithiol (pBDT) via disulfide bridges in aqueous environments and subsequently self-assembles with TA to form a coating (i.e., pBDT–TA) on various substrates (across nano-to-micrometer-scales) via the adherent properties of phenolics. [26,28] In contrast, monothiol-containing molecules do not result in robust coatings (Figure S1), indicating the importance of disulfide bridges for this coating method. This small molecule-mediated strategy allows for precise control over the coating thickness by varying the concentration of the BDT monomers. The π–π interactions between these building blocks can be leveraged to prepare highly stable coatings that resist harsh conditions, such as high salt environments (e.g., 100 mM NaCl), pH (e.g., pH 1 and pH 13), high temperatures (e.g., water at 100 °C), surfactant solution (e.g., 100 mM Triton X-100), and biological buffer (e.g., Dulbecco's phosphate-buffered saline (DPBS)), but can be selectively disassembled in certain organic solvents such as tetrahydrofuran (THF), dimethylformamide (DMF) and dimethyl sulfoxide (DMSO), as confirmed by experiments and simulations in the present study. The high stability of the coatings allows for diverse routes of modular postfunctionalization such as growth of a second material (e.g., ZIF-8 and polypyrrole) on the preformed pBDT–TA coatings. Additionally, aromatic dye molecules (e.g., rhodamine B) can be introduced into the coatings via π–π and/or π–cation interactions, endowing the coatings with tunable fluorescence properties (Figure 1b and c).

The coatings were prepared by mixing TA and BDT in bicine buffer (10 mM, pH 8.0) in the presence of substrates, (e.g., glass slides, Au substrates, silicon wafers, and polypropylene tubes). The colorless coatings were readily perceived by eye as the light reflection of the substrates changed after pBDT–TA deposition (Figure 2a and Figure S2), although bulk nucleation of pBDT–TA leading to a heterogeneous coating on the macroscopic scale was also observed. The pBDT–TA deposition was confirmed by scanning electron microscopy and energy-dispersive X-ray spectroscopy (EDX) (Figures S3–S6). Quartz crystal microbalance (QCM) measurements demonstrated the growth kinetics of the coating on a Au substrate where pBDT–TA grew continuously over 12 h (Figure 2b). Repeating the pBDT–TA deposition process allowed for the preparation of thicker films on a given substrate. For example, a 62 nm film (with a root-mean-square roughness of 12.8 nm) was obtained after two coating steps (Figure 2c and d). These results suggest the wide application range of the pBDT–TA coatings on diverse surfaces, from inorganic to organic, due to the near-universal adhesion of TA.[29]

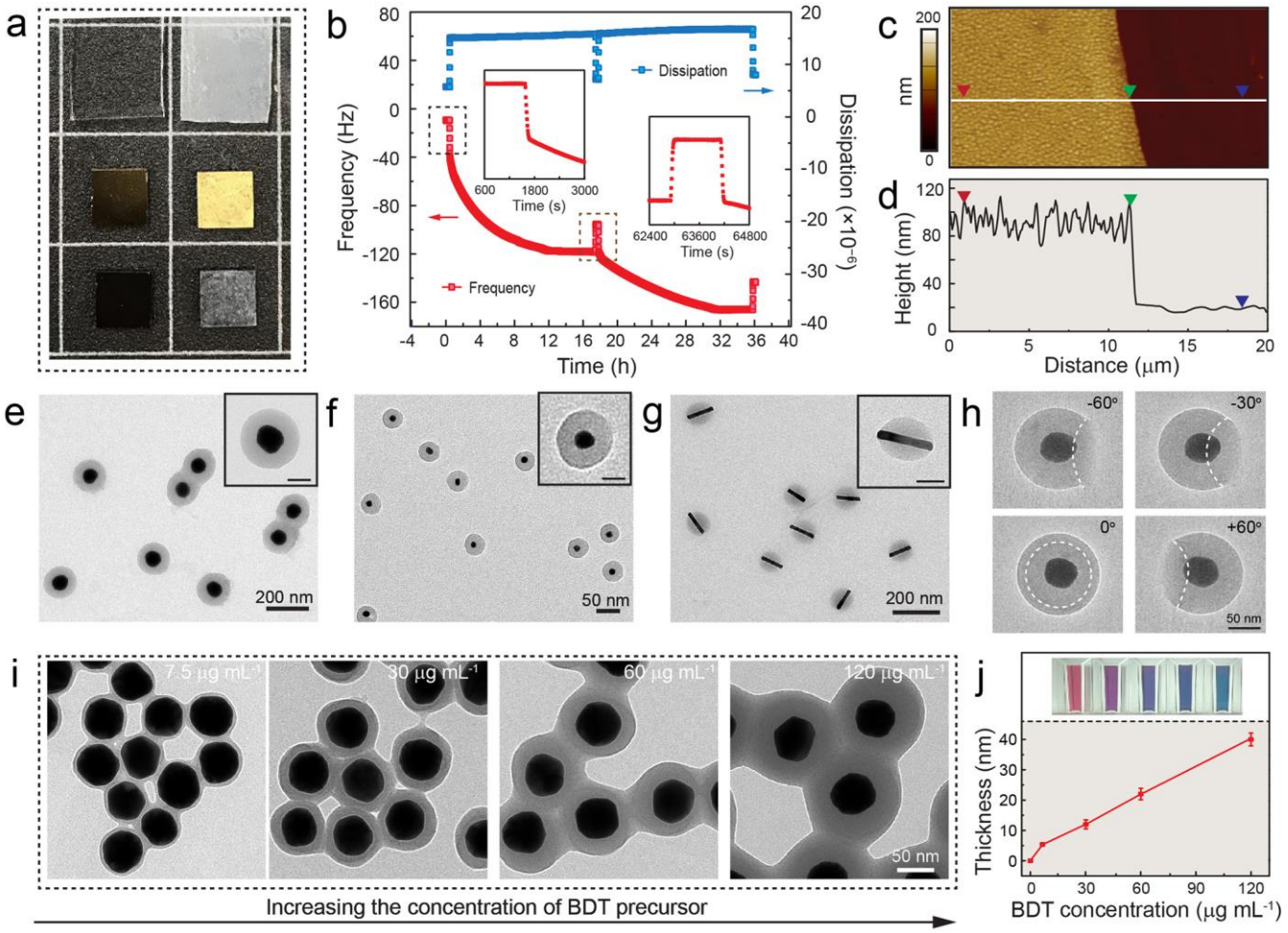

Figure 2. Formation of pBDT–TA coatings on various substrates. (a) Photographs of pBDT–TA coatings on various substrates. From top to bottom: glass, Au, and silicon wafers before (left) and after coating (right). The length of each white square is 1 cm. (b) Dynamic coating process of pBDT–TA complexes on a Au substrate, as monitored by QCM. The increased frequency at 18 h was due to a washing step. (c, d) Representative atomic force microscopy height image and corresponding height profile of the pBDT–TA coating on a Au substrate after two coating steps. (e–g) TEM images of pBDT–TA coatings on different nano-objects: 50 nm AuNPs (e), 14 nm AuNPs (f), and Au nanorods (g). Insets show the corresponding high-magnification TEM images of the coated nano-objects; scale bars are 50 nm (e, g) and 20 nm (f). (h) TEM images of Au@pBDT–TA viewed at different tilting angles. The white dashes indicate the boundary of the interface between pBDT and the TEM grid. (i) TEM images of AuNPs (50 nm) with different pBDT–TA coating thicknesses, as controlled by the concentration of BDT (7.5–120 μg mL^{-1}). (j) Relationship between the thickness of the coating and concentration of BDT monomers. Inset shows a photograph of AuNPs with different pBDT–TA coating thicknesses in solution.

The pBDT–TA coatings were also assembled on nanoscale substrates of different sizes and shapes (i.e., 50 nm Au nanoparticles (AuNPs), 14 nm AuNPs, 70 nm × 20 nm Au nanorods) (Figure 2e–g and Figure S7). For example, monodisperse 50 nm AuNPs were used to demonstrate the smooth and uniform pBDT–TA coating (Figure 2e). This was also confirmed by the dynamic light scattering (DLS) results—the Au@pBDT–TA displayed a narrow size distribution profile (Figure S8). Three-dimensional transmission electron microscopy (TEM) tomography further confirmed the uniformity of the pBDT–TA coating around the AuNPs (Figure 2h and Movie S1). The thickness of the pBDT–TA coatings was precisely controlled from 5 to 40 nm by simply increasing the amount of the BDT precursors used (Figure 3i and j). Owing to the colorless nature of this coating, an obvious redshift in the localized surface plasmon resonance (LSPR) of the Au@pBDT–TA nanoparticles was also observed (Figure 3j inset) from 535 nm (AuNPs) to more than 600 nm (Figure S9). Moreover, the thickness of pBDT–TA coatings can be modulated by varying the concentration of TA (Figure S10). Specifically, increasing the TA concentration led to a decrease in thickness.

We next investigated the stability of the pBDT–TA coatings. The DLS and UV–vis spectra results showed that the Au@pBDT–TA nanoparticles retained their original coating after incubation in various harsh aqueous environments (Figures 3a and S11) such as high salt environments (e.g., 100 mM NaCl), pH (pH 1 (HCl) and pH 13 (NaOH)), high temperatures (water at 100 °C), as well as surfactant solutions (e.g., 100 mM urea, 100 mM sodium dodecyl sulfate (SDS), 100 mM Triton X-100, and 100 mM Tween 20), and biological buffers (e.g., DPBS). TEM images further confirmed negligible changes in the thickness of the pBDT–TA coating under the above conditions (Figures 3b and S12). In contrast, the pBDT–TA coating was completely removed when incubated in THF, DMF, or DMSO. These results indicate the presence of π–π stacking in the supramolecular

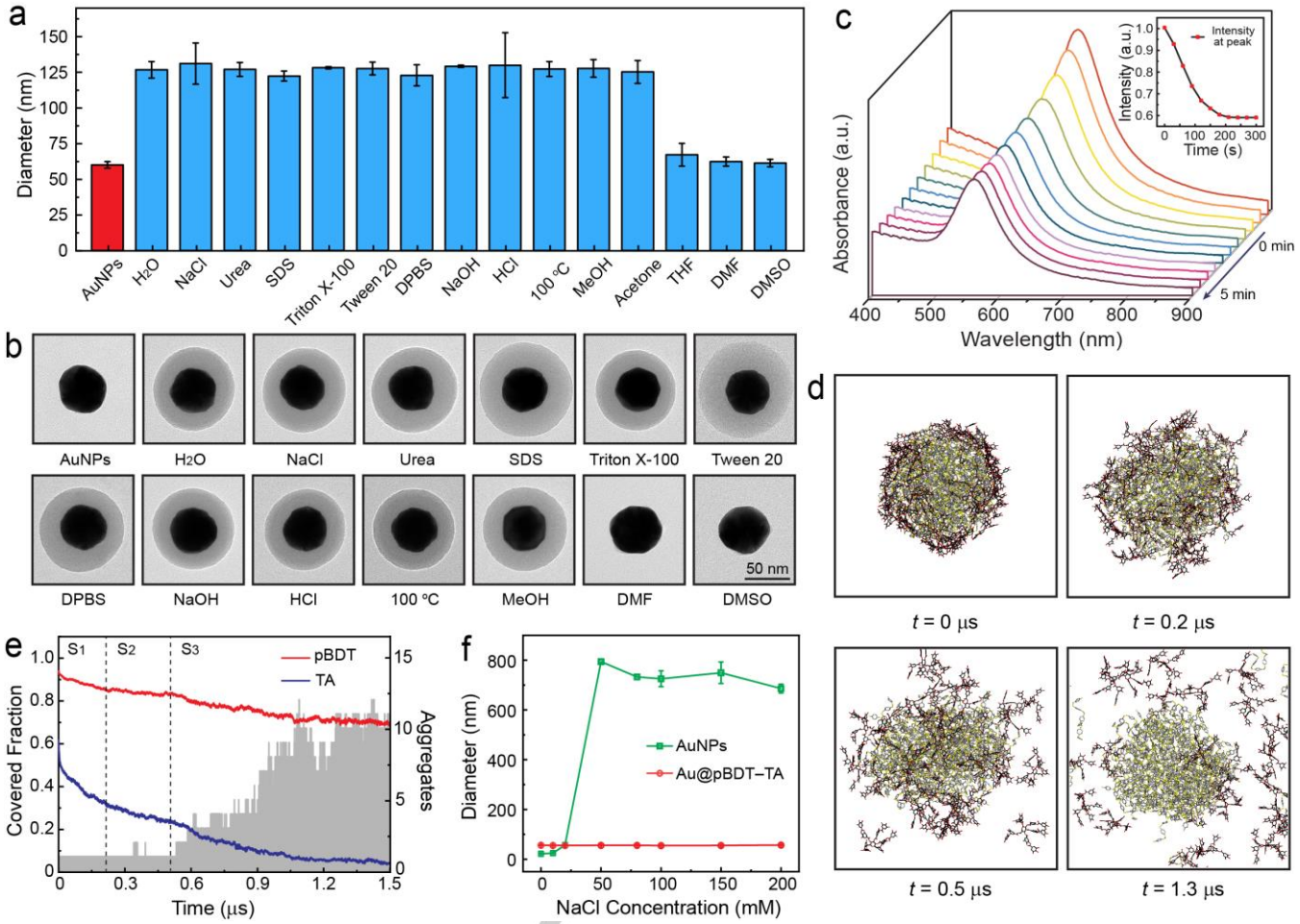

Figure 3. Stability of pBDT–TA coatings in different environments. (a) DLS results of the Au@pBDT–TA nanoparticles after incubation for 1 h in various media (including water at 100 °C). The concentration of NaCl, urea, SDS, Triton X-100, Tween 20, NaOH (pH 13), and HCl (pH 1) was 100 mM. (b) Representative TEM images of the Au@pBDT–TA nanoparticles after the different treatments. (c) UV–vis spectra of the Au@pBDT–TA nanoparticles in DMSO. Inset shows changes in intensity of the absorbance peak as a function of time. (d) Simulation snapshots of the complexes comprised of pBDT (yellow) and TA (red) measured in DMSO; the snapshots show disassembly at 0, 0.2, 0.5, and 1.3 μs. (e) Evolution of the covered fraction (i.e., fraction of molecules that are not accessible to the solvent) of pBDT (red) and TA (blue). The gray area represents the number of unconnected pBDT aggregates. (f) Colloidal stability of 14 nm AuNPs and pBDT–TA-coated AuNPs in response to different ionic strength (i.e., NaCl).

coating, which is consistent with our previous results.[26] The removal of the coating in DMSO as a function of time was monitored by UV–vis spectroscopy; the data showed that the pBDT–TA coating was effectively depleted within 5 min of incubation (Figure 3c).

All-atom molecular dynamics (MD) simulations were used to study the structural integrity of the pBDT–TA complexes in various solvents.[30] The aim of the MD simulations was to understand at a molecular level the mechanistic details of the disassembly of the pBDT–TA complexes in various solvents by modeling smaller TA–pBDT complexes, which mimic the structure of the larger (experimentally formed) coatings. The evolution of the radius of gyration (R_{gyr}) and the solvent-accessible surface area (SASA) of a pBDT–TA complex system immersed in different media (e.g., water, methanol (MeOH), DMSO, and DMF) was monitored and quantified (Figure 3d and e, and Figures S13–S17). The MD simulation results agreed with the experimental observations. Specifically, the complexes were stable in water (at 298 and 373 K) and MeOH and displayed varying degrees of disassembly in both DMSO and DMF on the time scales accessed by simulation.

The simulation studies revealed a three-stage disassembly mechanism (Figures 3e and S16 and S17): reorganization of the complex–solvent interface (Stage 1), TA dissociation (Stage 2), and pBDT core disassembly (Stage 3). Specifically, the annotated exemplar trajectory for the complex immersed in DMSO illustrates the progression and overlap of the stages of the disassembly mechanism (Figure 3e and S16). Stage 1 was observed between 0 to 0.2 μs where R_{gyr} of TA increased steadily as some of the aromatic "arms" of the TA molecules stretched from the complex to interact with DMSO. Stage 2 began at 0.2 μs where R_{gyr} of TA increased unsteadily as some of the TA molecules detached from the complex to be fully solvated in DMSO. In Stages 1 and 2, R_{gyr} of pBDT increased only slightly as the edges of the core "frayed". From 0.55 μs onwards, Stage 3 of the disassembly mechanism began as pBDT molecules detached from the core. This detachment is highlighted by a decrease in the covered fraction of both the

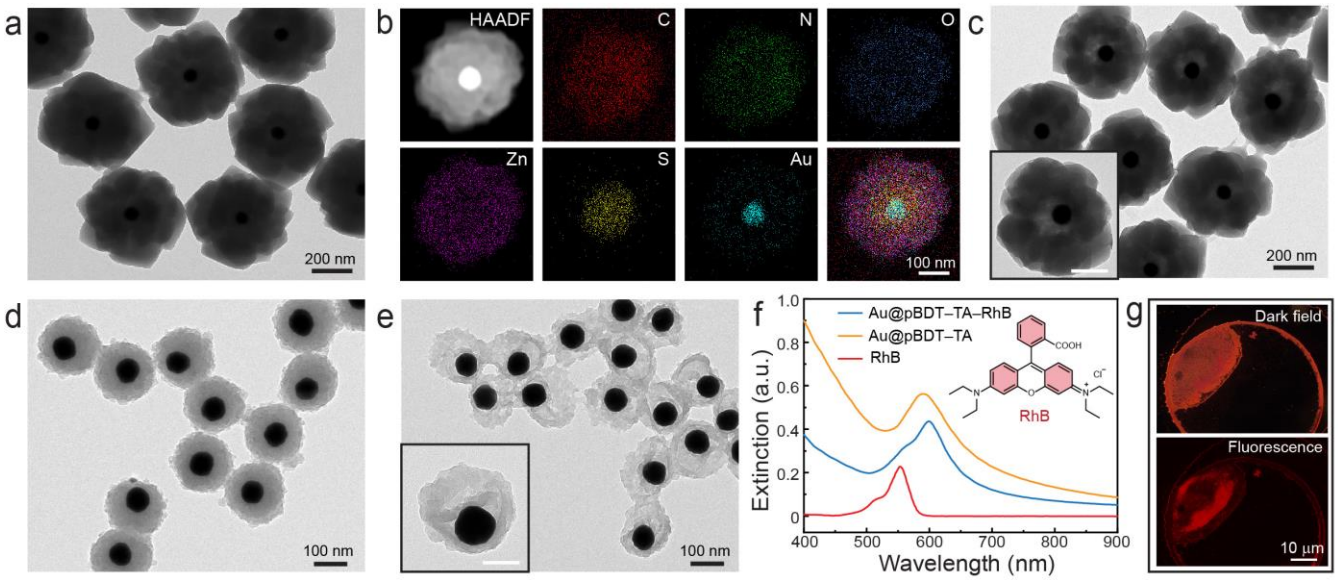

Figure 4. Functional modification of pBDT–TA-coated nanoparticles. (a, b) TEM image and EDX mapping of Au@pBDT–TA@ZIF-8. (c) Low-magnification and high-magnification (inset, scale bar is 100 nm) TEM images of Au@ZIF-8 yolk–shell structures. (d, e) TEM images of Au@pBDT–TA@PPy core–shell structures and Au@PPy yolk–shell structures. Inset image in (e): scale bar is 50 nm. (f) UV–vis extinction spectra of RhB, Au@pBDT–TA, and Au@pBDT–TA–RhB. (g) Dark-field and fluorescence images of Au@pBDT–TA–RhB nanoparticles.

core and TA (Figure 3e). In Stage 3, there was continued disassociation of TA from the pBDT core until most of the TA molecules were fully solvated in the DMSO (Figure 3d).

The simulations suggest that progression through the stages is dictated by the polarity of the solvent. Complexes in DMF also progressed through the three stages and the onset of core disassembly was observed (Figure S17). SASA evolution for the complexes of TA and pBDT in MeOH indicated significant interfacial reorganization of molecules with limited polyphenol disassociation, however, the steady R_{gyr} of pBDT indicates the absence of the third stage of the disassembly mechanism within the simulation time frame studied (Figure S15).

It is noted that the outermost layer of the pBDT–TA coating is composed of TA (Figure 3d), which is expected to give the coated nanoparticles improved colloidal stability.[31] Therefore, the colloidal stability of the pBDT–TA-coated nanoparticles was examined. AuNPs (14 nm) with a 15 nm pBDT–TA coating remained monodisperse without aggregation when dispersed in up to 200 mM NaCl (Figures 3f and S18). Such colloidal stability was in stark contrast with pristine AuNPs stabilized by citrate acid, which aggregated when the concentration of NaCl was above 20 mM (Figures 3f and S18). The improved colloidal stability was likely due to the electrostatic repulsive forces arising from the negative charge of the deprotonated phenolic groups (Figure S19), which also leads to steric hindrance from the hyperbranched structure of TA.[32–34]

The presence of TA on the surface can also act as a versatile platform for secondary reactions, leading to tailorable secondary coatings,[35] as the strong π–π interactions between pBDT and TA maintain the structure of the supramolecular network in different synthetic environments. For example, the pBDT–TA coating allowed for the deposition of uniform secondary layers of ZIF-8 in MeOH, yielding monodisperse core–shell particles (Figure 4a).[36] EDX mapping indicated the preservation of pBDT–TA networks underneath the ZIF-8 shell (Figure 4b). The pBDT–TA intermediate layer was removed after incubation in DMF to generate yolk–shell structures (Figure 4c). Similarly, polypyrrole (PPy) shells could be synthesized on the surface of the Au@pBDT–TA nanoparticles (Figure 4d), and complex yolk–shell structures were obtained by selectively removing pBDT–TA (Figure 4e). This platform exhibited flexibility in creating complex multimaterial nanostructures that are not easily accessible to other surface coating strategies.

The dominant π–π interactions in pBDT–TA also allowed for the integration of aromatic dyes into the coatings through π–π and/or π–cation interactions.[37] We employed a fluorescent dye (i.e., rhodamine B, RhB) to validate our design. RhB was mixed with BDT and TA in bicine buffer to co-assemble into supramolecular coatings (pBDT–TA–RhB) on AuNPs (Figure S20). The Au@pBDT–TA–RhB exhibited both the LSPR of Au and the characteristic absorbance peak of RhB (Figure 4f). The dye-labeled nanoparticles exhibited distinct fluorescence compared with Au@pBDT–TA (Figure S21), confirming the integration of the fluorescent RhB dye in the coatings. Moreover, the built-in Au cores can serve as additional contrast agents, as they have a high molar extinction coefficient and a scattering yield due to the LSPR.[38] Thus, this makes Au@pBDT–TA–RhB a dual-mode imaging probe—the scattering signal from the Au core and the fluorescent signal from the coating (Figure 4g).[39] Other aromatic dyes (e.g., rhodamine 19) can be also incorporated to tune the emission of these nanosystems (Figure S22). Such a platform could potentially be employed for tracking the fate of nanoparticles in bio–nano interactions and be used as multimodal imaging agents.[40,41]

In summary, the self-assembly of pBDT–TA coatings has been developed by exploiting π–π interactions between polyphenols and a self-polymerizable aromatic dithiol. These coatings can be assembled on diverse substrates in mild aqueous conditions with controllable thickness owing to the adhesive properties of the phenolic groups and the facile control of the supramolecular assembly. The strong π–π interactions promote stability of the coatings in various harsh environments (e.g., high ionic strength, high pH, high temperature, surfactant solution, and biological buffer), therefore allowing for secondary reactions under different synthetic conditions. Moreover, the pBDT–TA coatings enable the modular integration of aromatic fluorescent tags. This coating strategy is expected to expedite advances in functional supramolecular assemblies with potential in diverse fields.

Acknowledgements

We thank Dr. S. Pan, Mr. W. Yim, and Dr. H. Duan for helpful discussions. This research was conducted and funded by the Australian Research Council Centre of Excellence in Convergent Bio-Nano Science and Technology (project number CE140100036). F.C. acknowledges the award of a National Health and Medical Research Council Senior Principal Research Fellowship (GNT1135806). I.Y. and M.P. acknowledge computational resources provided through the National Computational Infrastructure (National Computational Merit Allocation Scheme grant e87) supported by the Australian Government. This work was performed in part at the San Diego Nanotechnology Infrastructure (SDNI) of University of California San Diego, a member of the National Nanotechnology Coordinated Infrastructure (NNCI), which is supported by the National Science Foundation (NSF) (Grant ECCS-1542148). J.V.J. acknowledges funding from the National Institutes of Health (DP2 HL137187) and NSF (1845683). R.P.M.L. acknowledges the Netherlands Organisation for Scientific Research for a Rubicon postdoctoral fellowship (project 019.182EN.034). J.J.R. acknowledges JSPS KAKENHI Grant Number 20F20373 and JSPS Fellowship P20373.

Keywords: functional self-assembly • nanostructures • polyphenols • supramolecular chemistry • surface engineering

[1] J. J. Richardson, M. Bjornmalm, F. Caruso, *Science* **2015**, *348*, aaa2491
[2] S. Clair, D. G. de Oteyza, *Chem. Rev.* **2019**, *119*, 4717–4776.
[3] R. R. Liu, J. Zhao, Q. Han, X. Y. Hu, D. Wang, X. Zhang, P. Yang, *Adv. Mater.* **2018**, *30*, 1802851.
[4] J. A. Berrocal, G. H. Heideman, B. F. M. de Waal, M. Enache, R. W. A. Havenith, M. Stohr, E. W. Meijer, B. Feringa, *J. Am. Chem. Soc.* **2020**, *142*, 4070–4078.
[5] A. V. Zhukhovitskiy, M. J. MacLeod, J. A. Johnson, *Chem. Rev.* **2015**, *115*, 11503–11532.
[6] J. Y. Park, L. R. Baker, G. A. Somorjai, *Chem. Rev.* **2015**, *115*, 2781–2817.
[7] J. Mosquera, Y. Zhao, H. J. Jang, N. L. Xie, C. L. Xu, N. A. Kotov, L. M. Liz-Marzan, *Adv. Funct. Mater.* **2020**, *30*, 1902082.
[8] H. A. Lee, Y. F. Ma, F. Zhou, S. Hong, H. Lee, *Acc. Chem. Res.* **2019**, *52*, 704–713.
[9] D. R. Lu, J. J. Zhou, S. Hou, Q. R. Xiong, Y. H. Chen, K. Y. Pu, J. H. Ren, H. W. Duan, *Adv. Mater.* **2019**, *31*, 1902733.
[10] Y. Wang, E. J. Jeon, J. Lee, H. Hwang, S. W. Cho, H. Lee, *Adv. Mater.* **2020**, *32*, 2002118.
[11] H. Lee, S. M. Dellatore, W. M. Miller, P. B. Messersmith, *Science* **2007**, *318*, 426–430.
[12] Z. E. Siwicka, F. A. Son, C. Battistella, M. H. Moore, J. Korpanty, N. C. McCallum, Z. Wang, B. J. Johnson, O. K. Farha, N. C. Gianneschi, *J. Am. Chem. Soc.* **2021**, *143*, 3094–3103.
[13] S. J. Pan, R. Guo, N. Bertleff-Zieschang, S. S. Li, Q. A. Besford, Q.-Z. Zhong, G. Yun, Y. T. Zhang, F. Cavalieri, Y. Ju, E. Goudeli, J. J. Richardson, F. Caruso, *Angew. Chem. Int. Ed.* **2020**, *59*, 275–280; *Angew. Chem.* **2020**, *132*, 281–286.
[14] Y. Y. Han, Z. Lin, J. J. Zhou, G. Yun, R. Guo, J. J. Richardson, F. Caruso, *Angew. Chem. Int. Ed.* **2020**, *59*, 15618–15625; *Angew. Chem.* **2020**, *132*, 15748–15755.
[15] H. Ejima, J. J. Richardson, K. Liang, J. P. Best, M. P. van Koeverden, G. K. Such, J. W. Cui, F. Caruso, *Science* **2013**, *341*, 154–157.
[16] J. J. Zhou, Z. Lin, Y. Ju, M. A. Rahim, J. J. Richardson, F. Caruso, *Acc. Chem. Res.* **2020**, *53*, 1269–1278.
[17] H. Su, W. J. Zhang, H. Wang, F. H. Wang, H. G. Cui, *J. Am. Chem. Soc.* **2019**, *141*, 11997–12004.
[18] W. Zhu, J. M. Guo, S. Amini, Y. Ju, J. O. Agola, A. Zimpel, J. Shang, A. Noureddine, F. Caruso, S. Wuttke, J. G. Croissant, C. J. Brinker, *Adv. Mater.* **2019**, *31*, 1900545.
[19] B. Hu, Y. Shen, J. Adamcik, P. Fischer, M. Schneider, M. J. Loessner, R. Mezzenga, *ACS Nano* **2018**, *12*, 3385–3396.
[20] T. Liu, M. K. Zhang, W. L. Liu, X. Zeng, X. L. Song, X. Q. Yang, X. Z. Zhang, J. Feng, *ACS Nano* **2018**, *12*, 3917–3927.
[21] Y. Ping, J. L. Guo, H. Ejima, X. Chen, J. J. Richardson, H. L. Sun, F. Caruso, *Small* **2015**, *11*, 2032–2036.
[22] Q. Wang, D. Astruc, *Chem. Rev.* **2020**, *120*, 1438–1511.
[23] Z. X. Wang, H. C. Yang, F. He, S. Q. Peng, Y. X. Li, L. Shao, S. B. Darling, *Matter* **2019**, *1*, 115–155.
[24] Z. L. Yu, F. Tantakitti, T. Yu, L. C. Palmer, G. C. Schatz, S. I. Stupp, *Science* **2016**, *351*, 497–502.
[25] G. Vantomme, E. W. Meijer, *Science* **2019**, *363*, 1396–1397.
[26] J. J. Zhou, Z. Lin, M. Penna, S. J. Pan, Y. Ju, S. Y. Li, Y. Y. Han, J. Chen, G. Lin, J. J. Richardson, I. Yarovsky, F. Caruso, *Nat. Commun.* **2020**, *11*, 4804.
[27] D. Wu, J. Zhou, M. N. Creyer, W. Yim, Z. Chen, P. B. Messersmith, J. V. Jokerst, *Chem. Soc. Rev.* **2021**, *50*, 4432–4483.
[28] P. Nowak, M. Colomb-Delsuc, S. Otto, J. W. Li, *J. Am. Chem. Soc.* **2015**, *137*, 10965–10969.
[29] M. A. Rahim, S. L. Kristufek, S. J. Pan, J. J. Richardson, F. Caruso, *Angew. Chem. Int. Ed.* **2019**, *58*, 1904–1927; *Angew. Chem.* **2019**, *131*, 1920–1945.
[30] Y. Y. Lin, M. Penna, M. R. Thomas, J. P. Wojciechowski, V. Leonardo, Y. Wang, E. T. Pashuck, I. Yarovsky, M. M. Stevens, *ACS Nano* **2019**, *13*, 1900–1909.
[31] Y. Y. Han, J. J. Zhou, Y. J. Hu, Z. X. Lin, Y. T. Ma, J. J. Richardson, F. Caruso, *ACS Nano* **2020**, *14*, 12972–12981.
[32] C. Zhang, D. F. Hu, J. W. Xu, M. Q. Ma, H. B. Xing, K. Yao, J. Ji, Z. K. Xu, *ACS Nano* **2018**, *12*, 12347–12356.
[33] J. L. Guo, T. Suma, J. J. Richardson, H. Ejima, *ACS Biomater. Sci. Eng.* **2019**, *5*, 5578–5596.
[34] W. T. Wang, H. Mattoussi, *Acc. Chem. Res.* **2020**, *53*, 1124–1138.
[35] J. L. Guo, B. L. Tardy, A. J. Christofferson, Y. L. Dai, J. J. Richardson, W. Zhu, M. Hu, Y. Ju, J. W. Cui, R. R. Dagastine, I. Yarovsky, F. Caruso, *Nat. Nanotechnol.* **2016**, *11*, 1105–1111.
[36] J. J. Zhou, P. Wang, C. X. Wang, Y. T. Goh, Z. Fang, P. B. Messersmith, H. W. Duan, *ACS Nano* **2015**, *9*, 6951–6960.
[37] S. Hong, Y. Wang, S. Y. Park, H. Lee, *Sci. Adv.* **2018**, *4*, eaat7457.
[38] A. M. Syed, S. Sindhwani, S. Wilhelm, B. R. Kingston, D. S. W. Lee, J. L. Gommerman, W. C. W. Chan, *J. Am. Chem. Soc.* **2017**, *139*, 9961–9971.
[39] F. Chen, P. Si, A. de la Zerda, J. V. Jokerst, D. Myung, *Biomater. Sci.* **2021**, *9*, 367–390.
[40] B. R. Kingston, A. M. Syed, J. Ngai, S. Sindhwani, W. C. W. Chan, *Proc. Natl. Acad. Sci. U. S. A.* **2019**, *116*, 14937–14946.

[41] D. Wu, J. J. Zhou, X. H. Chen, Y. H. Chen, S. Hou, H. H. Qian, L. F. Zhang, G. P. Tang, Z. Chen, Y. Ping, W. J. Fang, H. W. Duan, *Biomaterials* **2020**, *238*, 119847.

Entry for the Table of Contents

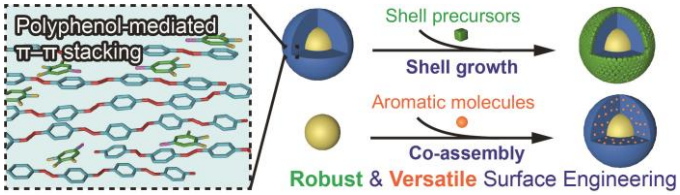

Interfacial assemblies are spontaneously formed on various substrates in aqueous conditions via simultaneous covalent and noncovalent interactions using tannic acid and the small aromatic molecule benzene-1,4-dithiol. The robust and colorless coatings enable the subsequent on-surface synthesis or modification for the development of various multifunctional coatings and nanosystems.